HOST DEFENSE

Itaconate is an effector of a Rab GTPase cell-autonomous host defense pathway against *Salmonella*

Meixin Chen[1]*, Hui Sun[1]*, Maikel Boot[1], Lin Shao[1], Shu-Jung Chang[1], Weiwei Wang[2], Tukiet T. Lam[2,3], Maria Lara-Tejero[1], E. Hesper Rego[1], Jorge E. Galán[1]†

The guanosine triphosphatase (GTPase) Rab32 coordinates a cell-intrinsic host defense mechanism that restricts the replication of intravacuolar pathogens such as *Salmonella*. Here, we show that this mechanism requires aconitate decarboxylase 1 (IRG1), which synthesizes itaconate, a metabolite with antimicrobial activity. We find that Rab32 interacts with IRG1 on *Salmonella* infection and facilitates the delivery of itaconate to the *Salmonella*-containing vacuole. Mice defective in IRG1 rescued the virulence defect of a *S. enterica* serovar Typhimurium mutant specifically defective in its ability to counter the Rab32 defense mechanism. These studies provide a link between a metabolite produced in the mitochondria after stimulation of innate immune receptors and a cell-autonomous defense mechanism that restricts the replication of an intracellular bacterial pathogen.

Many cells are endowed with the capacity to control microbial invaders through cell-intrinsic defense mechanisms that synergize with the immune system to confer whole-body protection (*1*). Microbial pathogens respond to these host defense strategies by evolving virulence factors that prevent their detection or neutralize the effects of the antimicrobial mechanisms (*2*). Rab-family guanosine triphosphatases (GTPases) coordinate molecular transport across cellular compartments (*3*). A member of this family, Rab32, orchestrates a cell-intrinsic host defense response that restricts the replication of intracellular bacterial pathogens, including *Salmonella enterica* serovar Typhi (*S.* Typhi) (*4*–*6*). *S. enterica* serovar Typhimurium (*S.* Typhimurium), however, can neutralize this restriction mechanism with two effectors (SopD2 and GtgE) delivered by its type III protein secretion systems (*7*, *8*). The mechanisms by which Rab32 controls bacterial replication are unknown. We hypothesized that Rab32 must control the delivery of an antimicrobial factor(s) to the *Salmonella*-containing vacuole (SCV). However, the nature of any potential factor(s) has remained elusive.

We searched for a cell line in which the Rab32-dependent restriction is robustly manifested by comparing the replication of wild-type *S.* Typhimurium with that of the Δ*gtgE* Δ*sopD2* mutant (deficient in both GtgE and SopD2), which is unable to neutralize it. We found no difference between the replication of the two strains in mouse embryo fibroblast, HeLa, or Henle-407 cells (Fig. 1, A to C), even after treatment with interferon (fig. S1). By contrast, we observed significant differences in murine DC2.4 dendritic cells (Fig. 1D) and, to a lesser extent, in RAW264.7 macrophages (Fig. 1E). Thus, the Rab32 phenotype may be more robustly manifested in cells of hematopoietic origin.

We then searched for Rab32-interacting proteins in DC2.4 cells after infection with the *S.* Typhimurium Δ*gtgE* Δ*sopD2* mutant strain at an infection time point that coincides with the recruitment of Rab32 to the SCV (*4*) (Fig. 1F). A prominent Rab32-interacting protein exclusively detected in infected cells was IRG1 (Fig. 1G and tables S1 and S2). This interaction was confirmed in cells expressing epitope-tagged versions of these proteins (Fig. 1H and fig. S2) and in DC2.4 cells expressing endogenous *Irg1* (Fig. 1I). The nucleotide state of Rab32 did not appear to affect its interaction with IRG1 (fig. S3). However, the interaction was enhanced by the bacterial infection (Fig. 1, H and I, and fig. S2). In addition, *IRG1* expression was detected in *Salmonella*-infected or lipopolysaccharide (LPS)–treated cells that showed the Rab32-restriction phenotype, but not in cells that did not (Fig. 1J and figs. S4 and S5). Furthermore, when compared with the wild-type strain, the *S.* Typhimurium Δ*gtgE* Δ*sopD2* mutant showed reduced intracellular replication in Henle-407 cells transiently expressing *IRG1* (fig. S6). IRG1, which is highly expressed in mouse macrophages after stimulation of Toll-like receptors (*9*), converts *cis*-aconitate, a tricarboxylic acid (TCA) cycle intermediate, to itaconic acid (*10*). By alkylating cysteine residues in the targeted molecules (*11*, *12*), itaconic acid (or itaconate) inhibits methylmalonyl–coenzyme A (CoA) mutase (*13*), as well as isocitrate lyase (*14*) and succinate dehydrogenase (*15*), which are essential enzymes in the glyoxylate shunt pathway and the TCA cycle. These pathways are critical for the physiology and pathogenesis of *Salmonella* and *Mycobacterium* spp. (*13*, *16*–*20*), which are susceptible to the Rab32-mediated defense mechanism (*4*, *7*, *21*). Furthermore, itaconic acid inhibits the growth of *Mycobacterium* spp., *S.* Typhimurium (*10*), and *S.* Typhi (fig. S7).

To investigate whether itaconic acid is delivered to the SCV, we developed a biosensor to report the presence of itaconic acid in *Salmonella*. *S.* Typhimurium encodes a putative itaconate-degradation pathway (*22*), which is absent from *S.* Typhi (Fig. 2A). By analogy to similar systems in other bacteria (*23*), expression of this pathway is expected to be controlled by a transcriptional regulatory protein (STM3121), which directly senses itaconic acid (Fig. 2A). We constructed a transcriptional reporter in which the expression of the green fluorescent protein (GFP), or nanoluciferase, was placed under the control of a promoter whose expression is directly controlled by STM3121 (Fig. 2A). The reporters responded to the presence of itaconic acid in a dose-dependent manner (Fig. 2, B and C), maintaining a linear response up to itaconate concentrations of ~5 to 6 mM (fig. S8). The reporter's response was specific because addition of other metabolites or environmental stimuli did not result in a measurable transcriptional response (fig. S9). We then tested whether itaconic acid was delivered to the SCV and whether the reporter strains could sense its presence within this environment. Infection of cells that do not express *IRG1* (Fig. 1) with *Salmonella* strains encoding the itaconate reporters did not result in any measurable production of nanoluciferase (Fig. 2D and figs. S10 and S11) or GFP (Fig. 2E and fig. S12). By contrast, infection of cells that express *IRG1* resulted in robust expression of the reporters (Fig. 2, D and E, and figs. S9 to S11). On the basis of the dose response of the reporter (fig. S8), the concentration of itaconate within the SCV was estimated to be ~6 mM, a concentration predicted to inhibit *Salmonella* growth (fig. S7).

We then examined whether the Rab32 pathway influences the production or the delivery of itaconate to the SCV. We reasoned that if the Rab32 pathway influences the presence of itaconate in the SCV, wild-type *S.* Typhimurium should impair this process by the action of SopD2 and GtgE (*4*, *7*). Consistent with this hypothesis, expression of the itaconate biosensor was detected at significantly reduced levels in DC2.4 or RAW264.7 cells infected with wild-type bacteria in comparison to the Δ*gtgE* Δ*sopD2* mutant strain (Fig. 3A and fig. S13), despite equivalent levels of *IRG1* expression in the infected cells (fig. S14). We then compared the expression of the itaconate reporter in bone marrow–derived macrophages (BMDMs) obtained from C57BL/6, *Irg1*$^{-/-}$, *Rab32*$^{-/-}$, or

[1]Department of Microbial Pathogenesis, Yale University School of Medicine, New Haven, CT 06536, USA. [2]WM Keck Foundation Biotechnology Resource Laboratory, Yale University School of Medicine, New Haven, CT 06536, USA. [3]Department of Molecular Biophysics and Biochemistry, Yale University School of Medicine, New Haven, CT 06536, USA.
*These authors contributed equally to this work.
†Corresponding author. Email: jorge.galan@yale.edu

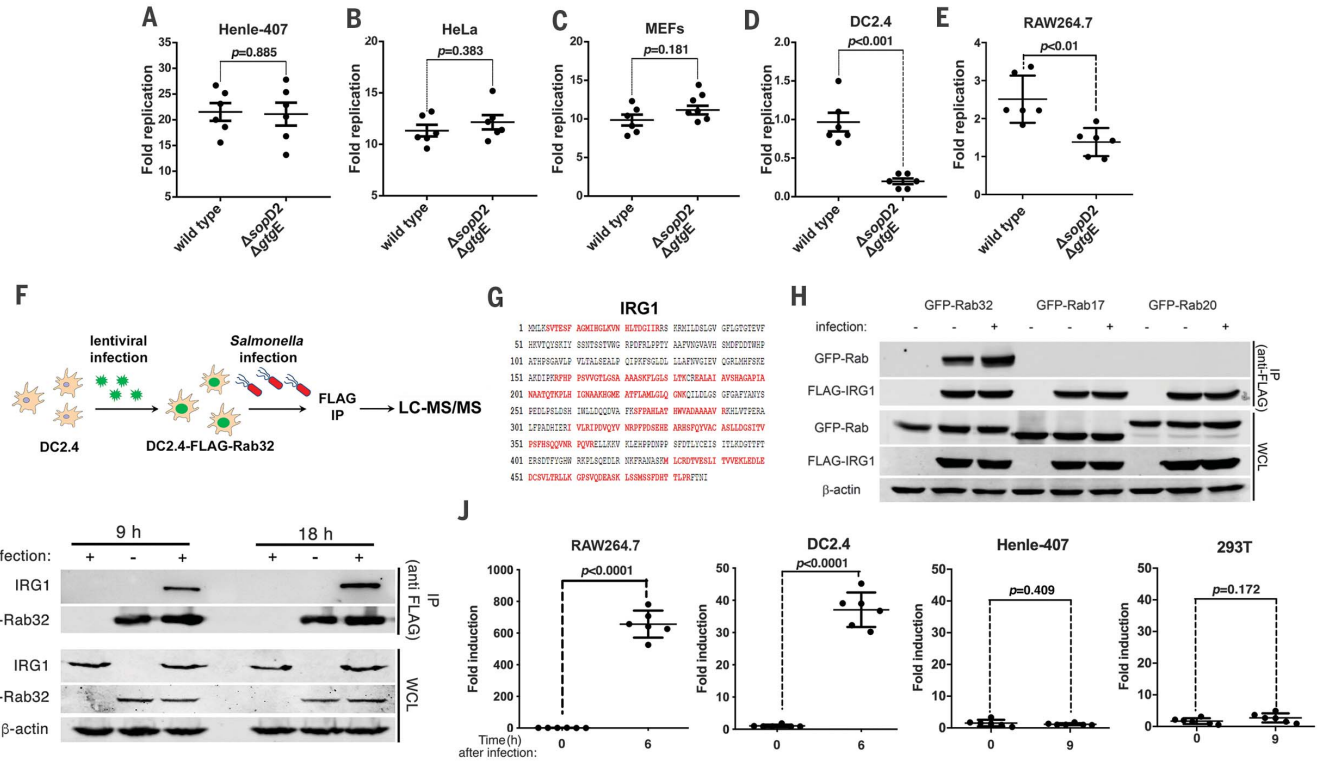

Fig. 1. IRG1 interacts with Rab32 during *Salmonella* infection. (**A** to **E**) The Rab32-associated pathogen restriction mechanism is manifested in myelocytic but not in epithelial cell lines. The ability of the *S.* Typhimurium Δ*sopD2* Δ*gtgE* mutant strain to replicate within epithelial [Henle-407 (A) and HeLa (B)], mouse embryonic fibroblast (MEF) (C), or myelocytic [DC2.4 (D) and RAW264.7 (E)] cell lines was evaluated by determining the colony forming units (CFU) at different times after infection [multiplicity of infection (MOI) = 5]. Fold replication represents the difference between the CFU at 1 and 9 hours after infection. Each circle represents the fold replication in each individual determination; the mean ± SEM of all the measurements and the *p* values of the indicated comparisons (two-sided Student's *t* test) are shown. (**F**) Rab32 interacts with IRG1 after *Salmonella* infection. DC2.4 cells expressing endogenous levels of FLAG-tagged Rab32 were infected with *S.* Typhimurium Δ*sopD2* Δ*gtgE* (MOI = 30), and Rab32-interacting proteins were identified by affinity purification and liquid chromatography–tandem mass spectrometry (LC–MS/MS) analysis. IP, immunoprecipitation. (**G**) The IRG1 peptides identified by the analyses in (F) are shown in red. Single-letter abbreviations for the amino acid residues are as follows: A, Ala; C, Cys; D, Asp; E, Glu; F, Phe; G, Gly; H, His; I, Ile; K, Lys; L, Leu; M, Met; N, Asn; P, Pro; Q, Gln; R, Arg; S, Ser; T, Thr; V, Val; W, Trp; and Y, Tyr. (**H** and **I**) Human embryonic kidney (HEK) 293T cells transiently cotransfected with a plasmid expressing GFP-tagged Rab32, Rab17, or Rab20, along with a plasmid encoding FLAG-tagged IRG1 (H), or DC2.4 cells stably expressing FLAG-tagged Rab32 (I) were infected with *S.* Typhimurium Δ*gtgE* Δ*sopD2* for 4 hours (MOI = 5). Cell lysates were then analyzed by immunoprecipitation with anti-FLAG and immunoblotting with anti-GFP, anti-FLAG, anti-IRG1, or anti–β-actin (as loading control) antibodies. IP, immunoprecipitates; WCL, whole-cell lysates. (**J**) Expression of *IRG1* after *Salmonella* infection. The indicated cell lines were infected with *S.* Typhimurium Δ*sopD2* Δ*gtgE* mutant strain (MOI = 5), and *IRG1* mRNA levels were measured by quantitative PCR 6 or 9 hours after infection. Each circle represents a single determination of the relative levels of *IRG1* normalized to the levels of glyceraldehyde-phosphate dehydrogenase (GAPDH); the mean ± SEM of all the measurements and *p* values of the indicated comparisons (two-sided Student's *t* test) are shown.

BLOC3-deficient (*Hps4*$^{-/-}$) mice, which lack the exchange factor for Rab32 (*24*), after infection with different *Salmonella* reporter strains. We found robust expression of the itaconate biosensor after infection of BMDMs obtained from C57BL/6 mice but not in BMDMs obtained from *Irg1*-defective mice (Fig. 3, B to D). Importantly, expression of the reporter was detected at significantly reduced levels in BMDMs obtained from *Hps4*$^{-/-}$ or *Rab32*$^{-/-}$ mice. Expression of the reporter in *Rab32*$^{-/-}$ BMDMs was higher than in *Hps4*$^{-/-}$ BMDMs, suggesting that in the absence of Rab32, the related Rab38 GTPase may partially compensate for its function (Fig. 3, B to D). The levels of itaconate in BMDMs obtained from C57BL/6, *Hps4*$^{-/-}$, or *Rab32*$^{-/-}$ mice after stimulation with LPS were indistinguishable from one another (Fig. 3E and table S3), indicating that the delivery of itaconate to the SCV, not its synthesis, is dependent on the Rab32-BLOC3 pathway.

A proportion of the intracellular *Salmonella* breaks from the SCV to the cell cytosol, where it can replicate at a faster rate (*25*). To investigate whether delivery of itaconate requires the integrity of the SCV, we examined the expression of the itaconate reporter in intravacuolar and cytoplasmic bacteria. Expression of the *S.* Typhi typhoid toxin requires the environment of the SCV, thus serving as a marker to distinguish intravacuolar versus intracytosolic bacteria (*26*). We found that all bacteria expressing the itaconate reporter were located within the SCV, whereas no bacteria found within the cytosol showed expression of the reporter (Fig. 3F and fig. S15).

The transport of mitochondria-originated products to other vesicular compartments is well documented (*27*, *28*). Because Rab32 is present in the mitochondria (*29*) and the SCV (*4*), this GTPase may aid the formation and/or delivery of itaconate and/or IRG1-transport carriers, or it may facilitate the tethering of the mitochondria with the SCV. We used live-cell

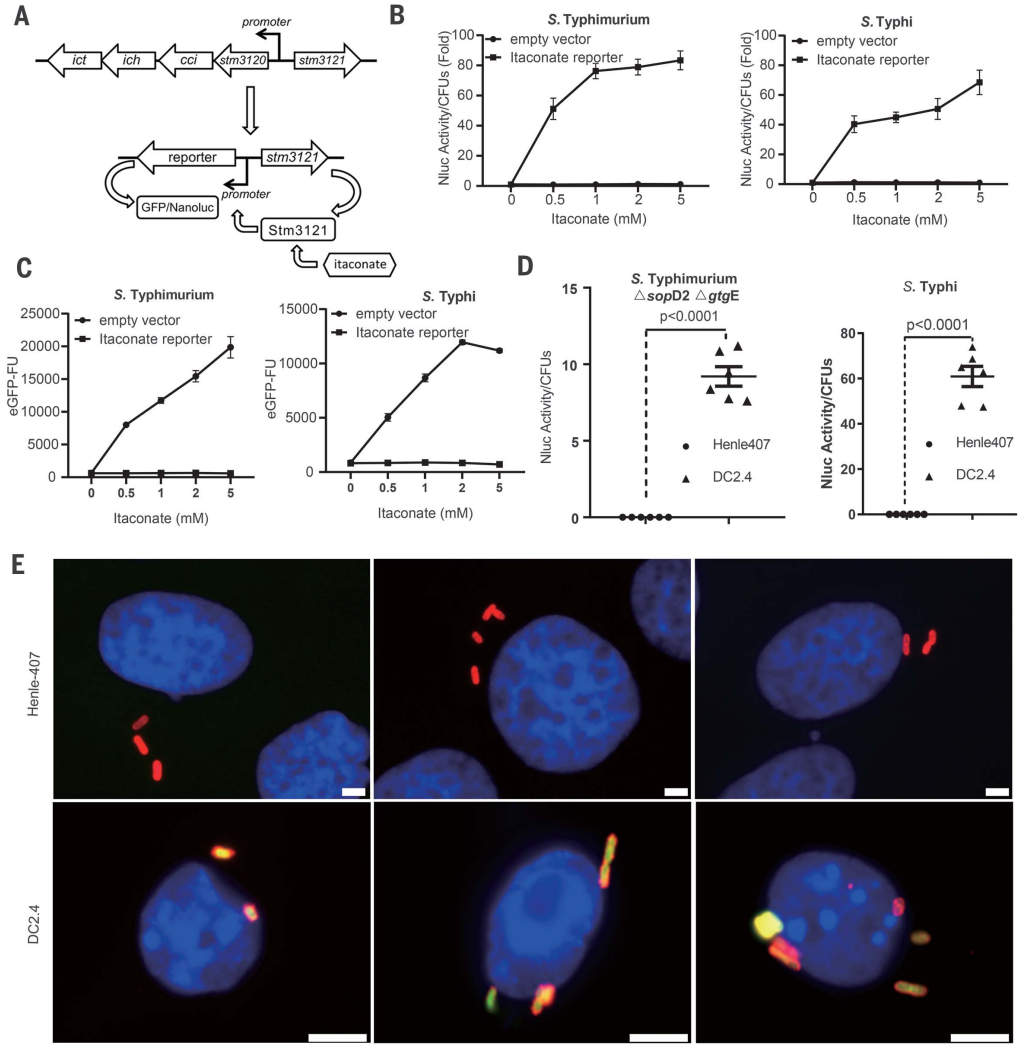

Fig. 2. Itaconate is delivered to the SCV. (**A** to **C**) Development of a biosensor to detect itaconate. The chromosomal organization of the itaconate-degradation gene cluster in *S.* Typhimurium and diagram of the itaconate biosensor are shown in (A). The effect of the addition of itaconate on the biosensor transcriptional response is shown in (B) and (C). *S.* Typhimurium and *S.* Typhi strains carrying either the nanoluciferase (Nluc) or enhanced GFP (eGFP) itaconate reporters were grown to an optical density at wavelength 600 nm (OD_{600}) of 0.9 in the presence of different concentrations of itaconic acid (as indicated), and the levels of nanoluciferase (B) or eGFP (C) were determined. Values are the mean ± SD of three independent measurements. This experiment was repeated at least three times with equivalent results. (**D** and **E**) Detection of itaconate by intracellular *Salmonella*. DC2.4 or Henle-407 cells were infected with *S.* Typhimurium Δ*sopD2* Δ*gtgE* mutant strain (MOI = 5) or *S.* Typhi (MOI = 10) carrying a plasmid encoding a nanoluciferase-based itaconate biosensor. Eighteen hours after infection, the levels of nanoluciferase were measured in lysates of the infected cells (D). Each circle or triangle represents a single luciferase measurement; the mean ± SD and *p* values of the indicated comparisons (two-sided Student's *t* test) are shown. This experiment was repeated at least three times with equivalent results. Alternatively, DC2.4 or Henle-407 cells were infected (MOI = 10) with *S.* Typhi carrying a plasmid encoding the eGFP-based itaconate biosensor (green). Eighteen hours after infection, cells were fixed, stained with 4′,6-diamidino-2-phenylindole (DAPI) (blue) to visualize nuclei and stained with an anti-*Salmonella* LPS antibody along with Alexa 594-conjugated anti-rabbit antibody (red), and imaged under a fluorescence microscope (E). Scale bars, 5 μm.

time-lapse fluorescence microscopy to examine cells stably expressing GFP-tagged IRG1 that had been infected with *Salmonella* expressing an mCherry itaconate reporter. We found that in uninfected cells, IRG1 was uniformly distributed throughout the entire mitochondrial network (fig. S16 and table S4). After *Salmonella* infection, we observed many instances in which the IRG1-containing mitochondrial network repositioned to surround and make intimate contact with the SCV, a process that coincided with the activation of the itaconate biosensor in the intracellular bacteria (Fig. 3G and movies S1 to S3). Examination of the infected cells by two-color three-dimensional super-resolution structured-illumination microscopy (3D-SIM) (*30*) revealed intimate contact between the IRG1-containing mitochondrial network and the SCV (Fig. 3H and movies S4 to S7). These observations suggest a mechanism by which the close association between the IRG1-containing mitochondria and the SCV may facilitate their tethering and subsequent itaconate transport.

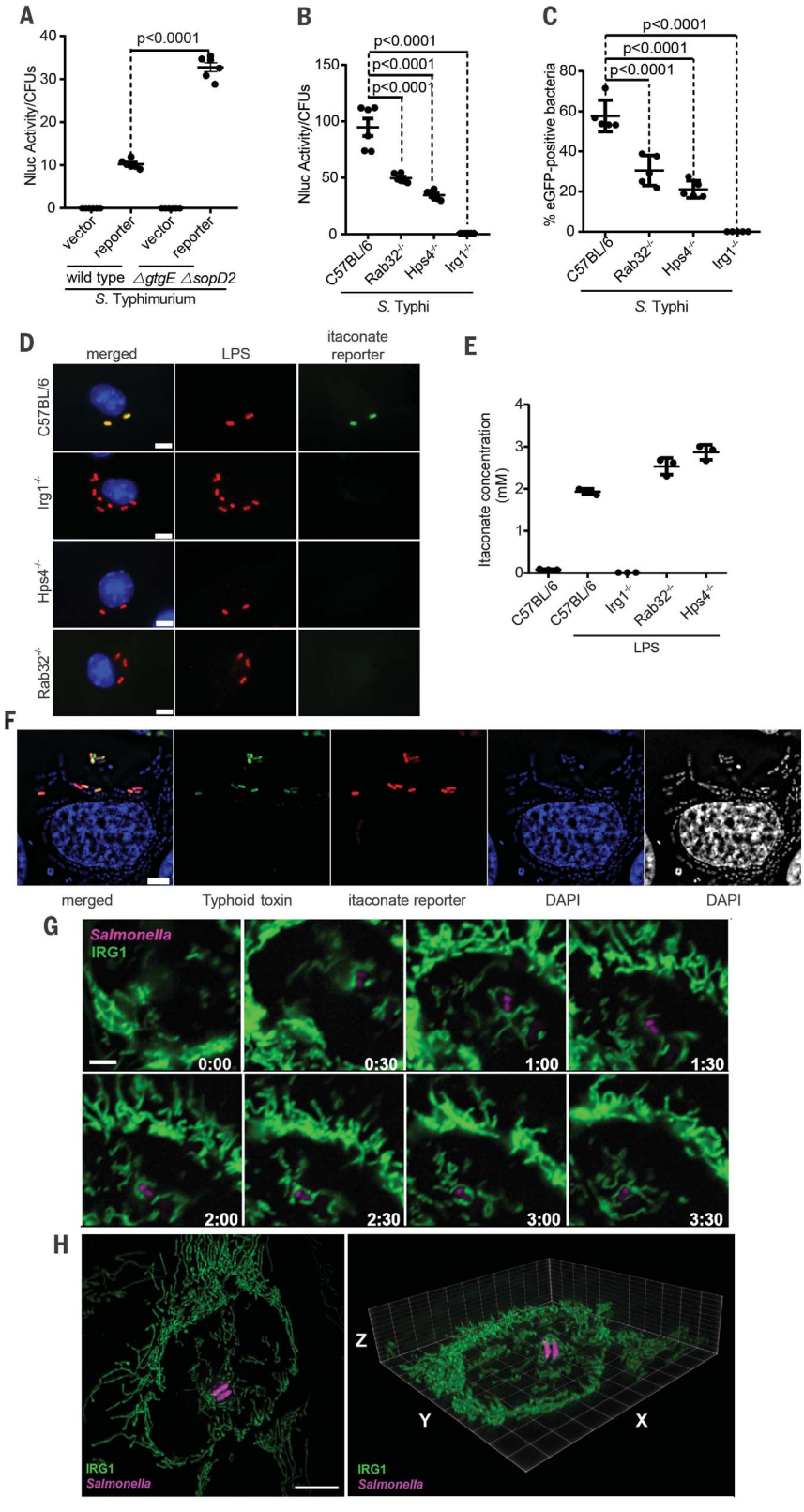

Fig. 3. Rab32-BLOC3–dependent delivery of itaconate to the SCV. (**A**) Cultured DC2.4 cells were infected with wild-type or Δ*gtgE* Δ*sopD2 S.* Typhimurium strains (MOI = 5) encoding the luciferase-based itaconate biosensor, and the levels of luciferase in cell lysates were measured 9 hours after infection. Each circle represents a single luciferase measurement; the mean ± SD and the *p* values of the indicated comparisons (two-sided Student's *t* test) are shown. (**B** to **D**) BMDMs obtained from C57BL/6, *Rab32*$^{-/-}$, *Hps4*$^{-/-}$, or *Irg1*$^{-/-}$ mice were infected with *S.* Typhi (MOI = 10) encoding the luciferase- or eGFP-based itaconate biosensors. Nine hours after infection, the levels of luciferase in cell lysates (B) or the number of cells expressing eGFP (C) were determined. Each circle in (B) represents a single luciferase measurement. Values in (C) represent the percentage of bacterial cells exhibiting fluorescence. A minimum of 200 cells in each condition were evaluated. The mean ± SD and *p* values of the indicated comparisons [one-way analysis of variance (ANOVA)] are shown. Representative fields of BMDMs obtained from the indicated mouse lines infected with *S.* Typhi encoding the eGFP itaconate reporter (green) are shown (D). Cells were fixed, stained with DAPI (blue) to visualize nuclei and stained with an anti-*Salmonella* LPS antibody along with Alexa 594-conjugated anti-rabbit antibody (red), and imaged under a fluorescence microscope. Scale bars, 5 μm. (**E**) Itaconate concentrations in BMDMs obtained from the indicated mice before and after LPS treatment to induce the expression of IRG1. Values represent the mean ± SD of three independent measurements. (**F**) Expression of the itaconate reporter (red) by intravacuolar but not by cytosolic *S.* Typhi. HeLa cells transfected with a plasmid encoding FLAG-tagged IRG1 were infected by a *S.* Typhi strain encoding an mCherry itaconate reporter (red) and a *pltB*::GFP transcriptional reporter (green). PltB, a component of the *S.* Typhi typhoid toxin, is exclusively produced by bacteria located within the SCV and therefore serves as a surrogate to report for intravacuolar (GFP^{+}) versus intracytosolic (GFP^{-}) bacteria. Six hours after infection, cells were stained with DAPI (to visualize all bacteria) and examined under a fluorescence microscope. Scale bars, 5 μm. (**G**) Live-cell fluorescence time-lapse microscopy of cultured HeLa cells stably expressing IRG1-GFP (green) infected with *S.* Typhimurium Δ*gtgE* Δ*sopD2* mutant strain encoding an mCherry itaconate biosensor (magenta). Imaging was initiated 45 min after infection. The times (hours:min) after initiation of imaging are indicated in each frame. (The entire sequence is shown in movie S1. This experiment was conducted at least three independent times, imaging several independent positions in each experiment, with equivalent findings. See movies S2 and S3 for additional examples.) Scale bar, 5 μm. (**H**) Snapshot of a 3D rendering of 3D-SIM acquisitions of HeLa cells stably expressing IRG1-GFP (green) infected with *S.* Typhimurium Δ*gtgE* Δ*sopD2* mutant strain encoding an mCherry itaconate biosensor (magenta). (Videos of this and additional reconstructions can be found in movies S4 to S7.) Scale bar, 5 μm.

We compared the ability of wild-type *S.* Typhimurium or the Δ*sopD2* Δ*gtgE* mutant to replicate within BMDMs obtained from C57BL/6, *Irg1*$^{-/-}$, or *Hps4*$^{-/-}$ mice. As previously shown (*7*), the *S.* Typhimurium Δ*sopD2* Δ*gtgE* mutant exhibited reduced ability to replicate within C57BL/6 BMDMs, and this phenotype was rescued in BMDMs obtained from *Hps4*$^{-/-}$ animals (Fig. 4A). Importantly, the replication-deficient phenotype was also rescued in BMDMs obtained from *Irg1*$^{-/-}$ mice, which allowed the replication of the

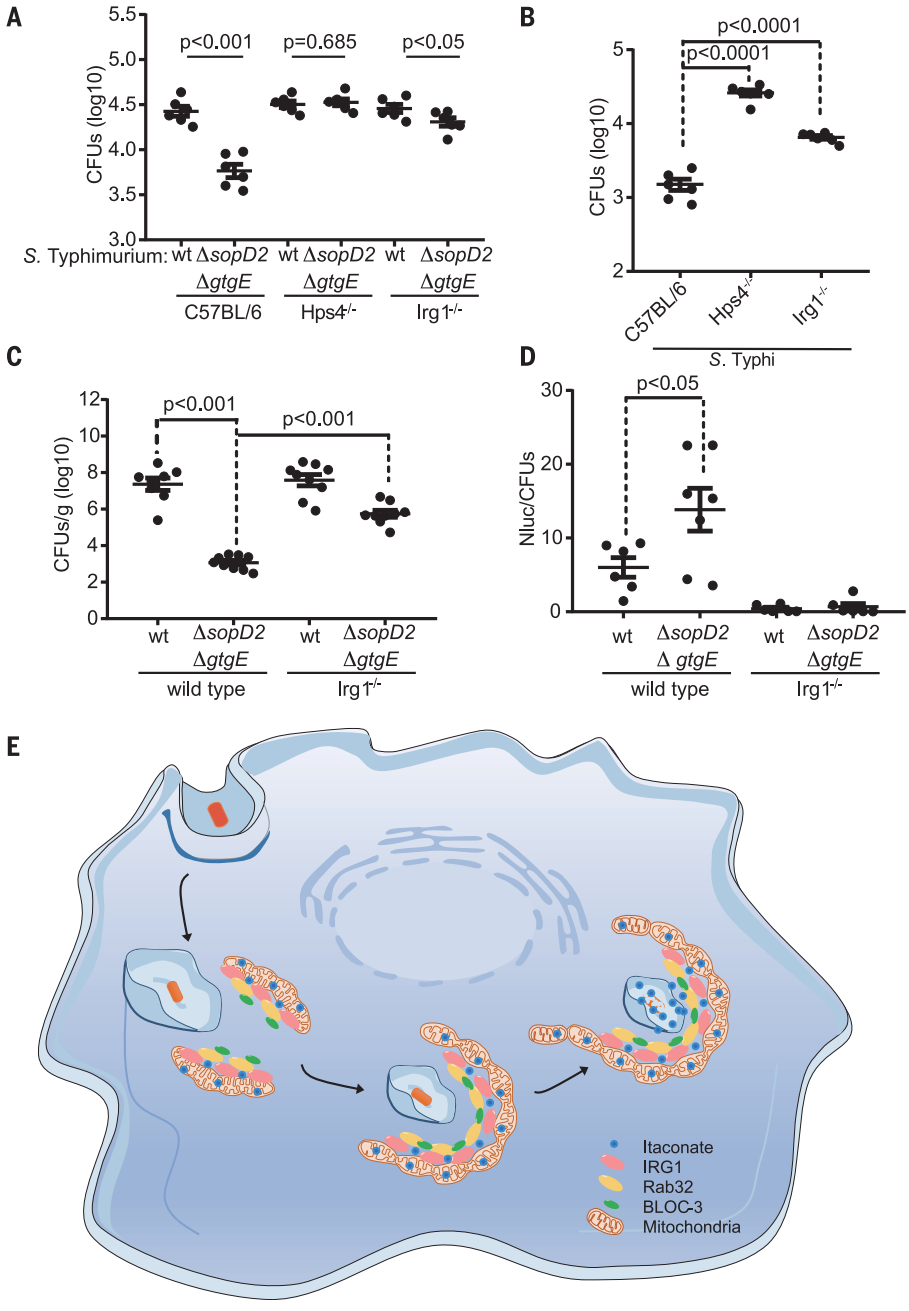

Fig. 4. Susceptibility of *IRG1*-deficient mice to *Salmonella* infection. (**A** and **B**) BMDMs obtained from C57BL/6 (wild-type), *Hps4*$^{-/-}$, or *Irg1*$^{-/-}$ mice were infected with wild-type (wt) *S.* Typhimurium (MOI = 5) or its Δ*gtgE* Δ*sopD2* mutant derivative (MOI = 5) (A) or wild-type *S.* Typhi (MOI = 10) (B), and the number of CFU was determined 9 hours after infection. Each circle represents the CFU in independent measurements; the mean ± SEM of all the measurements and *p* values of the indicated comparisons (two-sided Student's *t* test) are shown. (**C** and **D**) C57BL/6 (wild-type) or *Irg1*$^{-/-}$ mice were intraperitoneally infected with wild-type or Δ*gtgE* Δ*sopD2* *S.* Typhimurium (as indicated) (10^2 CFU). Five days after infection, bacterial loads in the spleen of the infected animals were determined (C). Alternatively, mice were intraperitoneally infected with the same strains (10^4 CFU), and the levels of luciferase activity in spleen lysates were quantified 24 hours after infection (D). Each circle in (C) represents the bacterial loads of the spleen of an individual animal, and each circle in (D) represents the luciferase levels in the spleen of an individual animal normalized to the CFU. The mean ± SEM of all the determinations and *p* values of the indicated comparisons (two-sided Student's *t* test) are shown. (**E**) Model for the mechanism of Rab32-BLOC3–mediated itaconate delivery to the SCV. On infection, the mitochondrial network repositions to surround the incoming bacteria, and the resulting close interaction between the mitochondria and the SCV results in the Rab32-BLOC3–dependent delivery of itaconate, which is synthesized in the mitochondria by IRG1.

S. Typhimurium Δ*sopD2* Δ*gtgE* mutant to levels almost equivalent to those of wild-type bacteria (Fig. 4A). The human-adapted pathogen *S.* Typhi is unable to replicate in mouse macrophages because the Rab32-BLOC3 pathway restricts its replication (*4*). As we have previously shown (*4*), *S.* Typhi was able to replicate in BMDMs from *Hps4*$^{-/-}$ mice to levels almost equivalent to those of wild-type *S.* Typhimurium (Fig. 4B). Importantly, *S.* Typhi was able to replicate in BMDMs from *Irg1*$^{-/-}$ mice, although not to the same extent as to the levels observed in BMDMs from *Hps4*$^{-/-}$ mice (Fig. 4B). This suggests that, in addition to itaconate, the Rab32-BLOC3 pathway may deliver additional antimicrobial factors. The *S.* Typhimurium Δ*sopD2* Δ*gtgE* mutant exhibits notably reduced mouse virulence when compared with the wild-type strain, and the virulence defect can be reversed in BLOC3-defective mice (*7*). We therefore reasoned that if itaconate is an effector of this pathway, the virulence attenuation of the *S.* Typhimurium Δ*sopD2* Δ*gtgE* mutant strain should be reversed in *Irg1*$^{-/-}$ mice. Consistent with this hypothesis, the virulence defect of the *S.* Typhimurium Δ*sopD2* Δ*gtgE* mutant was significantly reversed in *Irg1*$^{-/-}$ mice (Fig. 4C). We also examined whether the deployment of the SopD2 and GtgE effectors was able to blunt the delivery of itaconate to the SCV during infection. We found that 24 hours after infection, the itaconate reporter activity was almost undetectable in the spleens of animals infected with wild-type *S.* Typhimurium. By contrast, significantly higher activity was detected in the spleens of animals infected with the Δ*sopD2* Δ*gtgE* mutant strain (Fig. 4D).

We have shown here that itaconate is an effector of the Rab32-dependent pathogen restriction pathway that limits the replication of *Salmonella* (Fig. 4E). In phagocytic cells, itaconate can also be delivered to vacuoles containing other bacteria (e.g., *Escherichia coli*) or avirulent *S.* Typhi lacking its two type III secretion systems (fig. S17). We therefore hypothesized that this is a general mechanism of defense that may participate in the restriction of other vacuolar pathogenic bacteria. How itaconate inhibits bacterial growth is likely to be multifactorial, exerting its function by altering bacterial metabolism through its ability to inhibit key metabolic enzymes. Although itaconate has also been reported to have modulatory activities over multicellular responses, including inflammation (*31*), it is unlikely that those activities are central to the Rab32-BLOC3–mediated pathogen restriction mechanism, which involves the direct delivery of this metabolite to the bacterial-containing vacuole. These studies emphasize the critical role played by mitochondria in the control of microbial infections and the Rab32 pathway as a major link between this organelle

and the compartments housing bacterial pathogens.

REFERENCES AND NOTES

1. F. Randow, J. D. MacMicking, L. C. James, *Science* **340**, 701–706 (2013).
2. L. E. Reddick, N. M. Alto, *Mol. Cell* **54**, 321–328 (2014).
3. H. Stenmark, *Nat. Rev. Mol. Cell Biol.* **10**, 513–525 (2009).
4. S. Spanò, J. E. Galán, *Science* **338**, 960–963 (2012).
5. B. L. Tang, *Microbes Infect.* **18**, 595–603 (2016).
6. Y. Li *et al.*, *Immunity* **44**, 422–437 (2016).
7. S. Spanò, X. Gao, S. Hannemann, M. Lara-Tejero, J. E. Galán, *Cell Host Microbe* **19**, 216–226 (2016).
8. S. Spanò, X. Liu, J. E. Galán, *Proc. Natl. Acad. Sci. U.S.A.* **108**, 18418–18423 (2011).
9. C. G. Lee, N. A. Jenkins, D. J. Gilbert, N. G. Copeland, W. E. O'Brien, *Immunogenetics* **41**, 263–270 (1995).
10. A. Michelucci *et al.*, *Proc. Natl. Acad. Sci. U.S.A.* **110**, 7820–7825 (2013).
11. E. L. Mills *et al.*, *Nature* **556**, 113–117 (2018).
12. M. Bambouskova *et al.*, *Nature* **556**, 501–504 (2018).
13. M. Ruetz *et al.*, *Science* **366**, 589–593 (2019).
14. B. A. McFadden, S. Purohit, *J. Bacteriol.* **131**, 136–144 (1977).
15. T. Cordes *et al.*, *J. Biol. Chem.* **291**, 14274–14284 (2016).
16. R. B. Wilson, S. R. Maloy, *J. Bacteriol.* **169**, 3029–3034 (1987).
17. F. C. Fang, S. J. Libby, M. E. Castor, A. M. Fung, *Infect. Immun.* **73**, 2547–2549 (2005).
18. J. D. McKinney *et al.*, *Nature* **406**, 735–738 (2000).
19. R. Mercado-Lubo, E. J. Gauger, M. P. Leatham, T. Conway, P. S. Cohen, *Infect. Immun.* **76**, 1128–1134 (2008).
20. T. Hartman *et al.*, *PLOS Pathog.* **10**, e1004510 (2014).
21. F. Zhang *et al.*, *Nat. Genet.* **43**, 1247–1251 (2011).
22. J. Sasikaran, M. Ziemski, P. K. Zadora, A. Fleig, I. A. Berg, *Nat. Chem. Biol.* **10**, 371–377 (2014).
23. E. K. R. Hanko, N. P. Minton, N. Malys, *ACS Synth. Biol.* **7**, 1436–1446 (2018).
24. A. Gerondopoulos, L. Langemeyer, J. R. Liang, A. Linford, F. A. Barr, *Curr. Biol.* **22**, 2135–2139 (2012).
25. L. A. Knodler, *Curr. Opin. Microbiol.* **23**, 23–31 (2015).
26. C. C. Fowler, J. E. Galán, *Cell Host Microbe* **23**, 65–76.e6 (2018).
27. G. Soto-Heredero, F. Baixauli, M. Mittelbrunn, *Front. Cell Dev. Biol.* **5**, 95 (2017).
28. B. H. Abuaita, T. L. Schultz, M. X. O'Riordan, *Cell Host Microbe* **24**, 625–636.e5 (2018).
29. N. M. Alto, J. Soderling, J. D. Scott, *J. Cell Biol.* **158**, 659–668 (2002).
30. M. G. Gustafsson *et al.*, *Biophys. J.* **94**, 4957–4970 (2008).
31. X. H. Yu, D. W. Zhang, X. L. Zheng, C. K. Tang, *Immunol. Cell Biol.* **97**, 134–141 (2019).

ACKNOWLEDGMENTS

We thank M. Diamond and M. Artyomov for providing the *Irg1*$^{-/-}$ mouse. **Funding:** The Proteomics Resource of the W.M. Keck Foundation Biotechnology Resource Laboratory was partially supported by CTSA grant number UL1TR001863 from the National Center for Advancing Translational Sciences (NCATS) of the National Institutes of Health (NIH). This work was supported by NIH grants R01AI114618 and R01AI055472 to J.E.G. E.H.R. is supported by the Pew Biomedical Research Program and the Searle Scholars Program. M.B. is supported by an EMBO long-term fellowship. **Author contributions:** M.C. performed most of the experiments, H.S. performed initial experiments, M.B. and L.S. carried out the imaging studies, S.-J.C. assisted M.C. in some experiments, W.W. and T.T.L. performed the itaconate measurements, M.L.-T. performed the LC-MS/MS experiments, E.H.R. supervised the imaging experiments, and J.E.G. conceived and directed the project and wrote the manuscript with comments from all the authors. **Competing interests:** The authors declare no competing interests. **Data and materials availability:** All data are available in the main text, supplementary materials, and auxiliary files.

SUPPLEMENTARY MATERIALS

science.sciencemag.org/content/369/6502/450/suppl/DC1
Materials and Methods
Figs. S1 to S17
Tables S1 to S5
References (*32*–*36*)
Movies S1 to S7

View/request a protocol for this paper from *Bio-protocol*.

14 August 2019; resubmitted 26 January 2020
Accepted 15 May 2020
10.1126/science.aaz1333

Science

Itaconate is an effector of a Rab GTPase cell-autonomous host defense pathway against *Salmonella*

Meixin Chen, Hui Sun, Maikel Boot, Lin Shao, Shu-Jung Chang, Weiwei Wang, Tukiet T. Lam, Maria Lara-Tejero, E. Hesper Rego and Jorge E. Galán

Science **369** (6502), 450-455.
DOI: 10.1126/science.aaz1333

Rab32 puts itaconate where it's needed

Myeloid cells can restrict the replication of intracellular bacterial pathogens such as *Salmonella* using a Rab family guanosine triphosphatase called Rab32. However, the underlying mechanisms remain unclear. Chen *et al.* report that Rab32 and its exchange factor, BLOC3, interact with aconitate decarboxylase 1 (IRG1). This complex enables the direct delivery of IRG1's antimicrobial product, itaconate, from the mitochondria to *Salmonella*-containing vacuoles. Itaconate concentrations in vacuoles correlated with bacterial survival, highlighting the biological relevance of this metabolite during infections. Similar findings in *Escherichia coli*–infected cells suggest that this is a more general phenomenon in which mitochondria and the Rab32 pathway play a critical role in antibacterial host defense.

Science, this issue p. 450